Preparation and Characterization of K_2CO_3-Activated Kraft Lignin Carbon

Xian-fa Li,[a,*] Xue-gang Luo,[b] Lin-qin Dou,[a] and Ke Chen [a]

A series of activated carbons (ACs) were prepared by K_2CO_3 activation from kraft lignin (KL) that was recovered from papermaking black liquor. The effects of process parameters such as the activation temperature (AT), activated period, K_2CO_3 to KL mass ratio, and N_2 flow rate on the characteristics of the final product were determined. The ACs were characterized using nitrogen adsorption, morphology, and fractal dimension analyses. The results showed that the AT was the main factor influencing the yield, surface area, and pore structure. The yield of ACs obviously decreased from 50.6% to 20.5% with increasing AT from 600 °C to 1000 °C, and decreased with increasing K_2CO_3/KL mass ratio. Activation time and N_2 flow rate had slight effect on the yield of ACs. The surface area and total pore volume increased as the AT rose to 900 °C and then decreased with further increases in temperature. The maximum surface area and total pore volume were 1816.3 m^2/g and 1.26 cm^3/g, respectively, at a K_2CO_3 to KL mass ratio of 3:1, AT of 900 °C, activation time of 2 h, and N_2 flow rate of 70 cm^3/min. The pore structure of the ACs could be tailored by controlling the AT. As the AT was increased from 700 to 1000 °C, the mesoporosity increased from 11.6% to 95.9%. SEM images indicated that the morphology of ACs was modified by the AT. The K_2CO_3 was partially recycled.

Keywords: Kraft lignin; K_2CO_3; Chemical activation; Activated carbon; Structural characterization

*Contact information: a: School of Life Science and Engineering, Southwest University of Science and Technology, Mianyang 621010, China; b: Engineering Research Center of Biomass Materials (SWUST), Ministry of Education, Mianyang 621010, China; *Corresponding author: lixianfa@swust.edu.cn*

INTRODUCTION

Activated carbon (AC) is the most popularly used absorbent for gas- and liquid-phase applications, and also for capacitor and catalyst support products (Zhang *et al*. 2014a; Li *et al*. 2015). Due to its low cost and renewability, the biomass from industrial wastes, agricultural, or forestry by-products, as a precursor for AC production, has received much attention (Liu *et al*. 2015; Jain *et al*. 2016). Lignin is the second most abundant natural polymer and most abundant phenolic polymer with substituted phenylpropane units, that represents a major component of non-edible biomass (Bu *et al*. 2012). Lignin contributes as much as 30% of the weight and as much as 40% of the energy content of lignocellulosic biomass (Lange *et al*. 2013). Kraft lignin (KL) is a byproduct of biomass pulping; most KL is now directly burned to generate energy, which is a disadvantage because the storage of fuel is often complicated and oftentimes requires immediate use. Moreover, the emission of flammable gas and ash could result in environmental problems (Kang *et al*. 2013). Because KL has a high carbon content, it is a suitable precursor for the preparation of activated carbon (Suhas *et al*. 2007).

A few studies used chemical activation with KOH, NaOH, K_2CO_3, Na_2CO_3, H_3PO_4 or $ZnCl_2$, and physical activation with CO_2 or steam to prepare KL-ACs (Carrott et al. 2008; Torné-Fernández *et al*. 2009; Huang *et al*. 2014; Saha *et al*. 2014). Among the alkaline chemical activating agents, KOH and K_2CO_3 are preferred (Babel and Jurewicz 2008; Xia *et al*. 2015). Hayashi *et al*. (2000) examined the influence of the activating reagents K_2CO_3 and KOH on the pore structure of KL-ACs. The results indicated that the surface area and pore volume of K_2CO_3 activated AC exceeded that of carbon activated with KOH at the same activation temperature. Moreover, both ACs were mainly microporous carbon. Foo *et al*. (2011) used rice husks as a feedstock for preparation of activated carbon by microwave induced KOH and K_2CO_3 activation. Their results revealed that the K_2CO_3-activated sample showed higher yield and better pore structures and adsorption capacity development than the KOH-activated sample. These studies focused on the characteristics of the final product such as the surface area, pore volume and pore size distribution. However, very few studies have involved the tailored mesopore AC preparation, fractal dimension characterization of AC, and activating agent recovery (Song *et al*. 2012; Li *et al*. 2014). Moreover, KOH as an activating agent has some disadvantages, such as a strong erosion rate, high cost, and low carbon yield. Compared with KOH, K_2CO_3 is less expensive and capable of green recycling (Liu *et al*. 2012).

In the present work, KL-activated carbons were prepared using a simple, one-step K_2CO_3 activation method, as shown in Fig. 1. After activation, a portion of K_2CO_3 was recovered from the washing water by crystallization, and some of the washing water was reused as primary washing water so that the emission of alkaline washing wastewater could be reduced. The influence of the activation temperature, mass ratio of K_2CO_3 to Kraft lignin, activation time, flow rate of N_2 gas on the carbon yield, specific surface area, and pore structure of the activated carbons was investigated.

EXPERIMENTAL

Materials and Reagents

Industrial-grade KL was purchased from the Xuemei Paper Mill in Shandong Province (Shandong, China) and was used for an acid de-ash pretreatment. Analytical-grade H_2SO_4 (98%) and K_2CO_3 were purchased from the Sinopharm Chemical Reagent Co. (Chengdu, China). High-purity N_2 was obtained from the Mianyang Special Gases Factory (Minyang, China).

Preparation of the ACs

The acid de-ash pretreatment process of KL, based on previous literature (Fierro *et al.* 2007), was used to prepare the deash KL (KL_d). The activation process of KL_d is shown in Fig. 1. During the activation procedure, 5.0 g of KL_d was physically mixed with powdery K_2CO_3 using various K_2CO_3 to KL_d mass ratio of 1:1, 2:1, 3:1, and 4:1. The mixed sample was set on a ceramic boat that was then inserted into a stainless steel reaction tube (diameter of 50 mm). The carbonization and activation of KL_d were carried out in a horizontal tube furnace flushed with nitrogen. The activation conditions are as follows: heating rate of 10 °C/min, activation temperature of 600 to 1000 °C, activation time of 1 to 3 h, and N_2 flow rate of 40 to 100 cm^3/min. At the end of activation, the samples were cooled down under same N_2 flow rate. The activated samples were preliminarily washed repeatedly with 50 mL of circulating water for three times and separated according to solid and filtrate portions.

The three incorporative filtrate was concentrated by rotation distillation and crystallized to recover the K_2CO_3. The solid portion was washed with distilled water until it had been neutralized. The washed samples were dried at 105 °C for 12 h and then ground to form the activated carbon powder.

ACs Characterization

The surface area, pore volume, and pore diameter were determined from the corresponding nitrogen adsorption-desorption isotherms obtained at 77 K with an automatic instrument (TriStar II 3020 V1.03, Micromeritics, Norcross, GA, USA). Prior to the adsorption measurements, all samples were outgassed in a vacuum at 300 °C for 300 min. The specific surface area was calculated using the Brunauer-Emmett-Teller (BET) method, and the total pore volume was calculated using the adsorption data at a relative pressure of 0.973. The micropore area and volume and the mesopore surface area were obtained from the t-plot method. The average pore diameter was calculated from the N_2 adsorption isotherm using the Barrett-Joyner-Halenda (BJH) method.

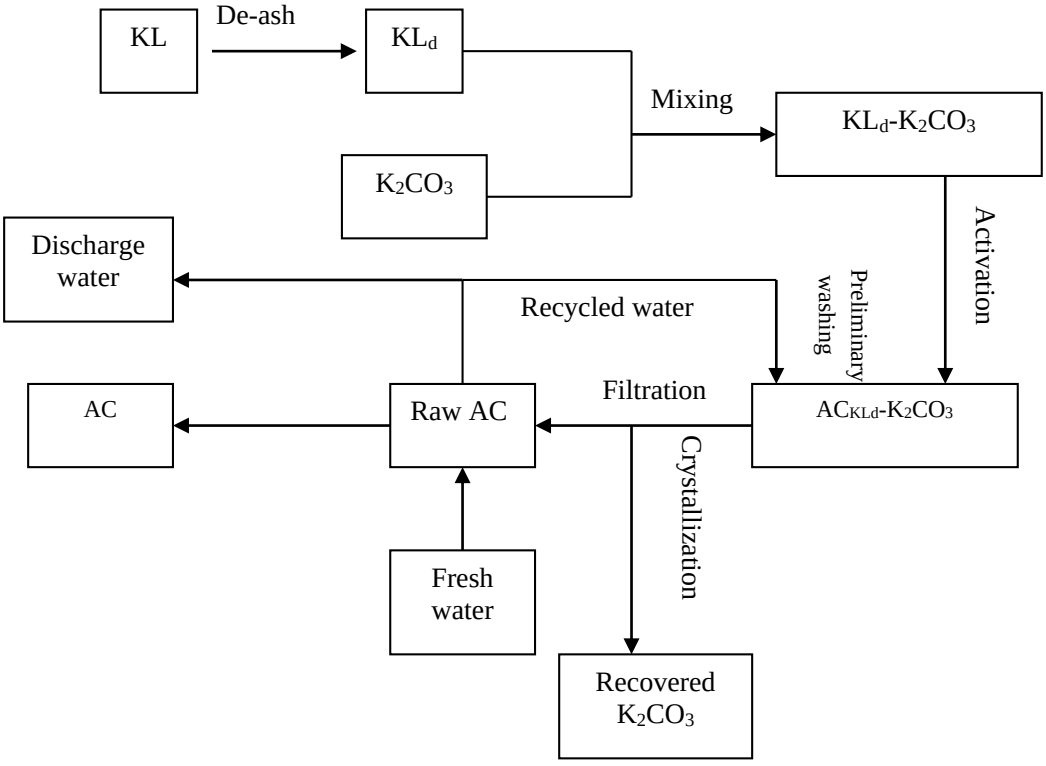

Fig. 1. Schematic of the preparation of ACs from KL_d by K_2CO_3 activation

The surface morphologies of the ACs were imaged using a scanning electron microscope (SEM) (Model JSM-6700F, JEOL Ltd., Tokyo, Japan).

The recovery ratio of K_2CO_3 was calculated using Eq. 1,

$$Recovery\% = \frac{m_1 - m_{AC}}{m_2} \times 100\% \quad (1)$$

where *Recovery%* is recovery ratio of K_2CO_3, m_1 is the mass of AC_{KLd}-K_2CO_3 mixture after activation and before washing, m_{AC} is the final AC mass, and m_2 is the initial K_2CO_3 mass.

The fractal dimension, which is a measurement of roughness or irregularity, was determined by applying the following Frenkel-Halsey-Hill (FHH) equation (Hayashi *et al*. 2002) to the N_2 adsorption isotherm on ACs at 77 K.

$$V = K[\ln\left(\frac{P_0}{P}\right)]^{D-3} \quad (2)$$

where V is the liquid nitrogen amount adsorbed by filling micropore volume at a relative pressure (P/P_0) between 0.0 and 0.3, P_0 is saturation pressure, P is adsorption pressure, K is a constant, and D is the fractal dimension. The logarithm of the amount adsorbed (V) and the logarithm of $\ln(P_0/P)$ are shown in the FHH plot. The linear behavior and the fractal dimension (D) make up the slope.

RESULTS AND DISCUSSION

The effect of the activation temperature on the carbon yield is shown in Table 1 (entries 1 to 5). The results revealed that the yield decreased from 50.6% to 20.5% when the activation temperature was increased from 600 to 1000 °C. A higher activation temperature released more volatiles and therefore reduced the carbon yield.

Table 1. Textural Characteristics of ACs Obtained by K_2CO_3 Activation

Entry	$AC_{R\text{-}T\text{-}t\text{-}v}$ [1]	A_{BET} [2] (m^2/g)	A_e [3] (m^2/g)	Mesopore proportion (%)	V_t [4] (cm^3/g)	V_{micro} [5] (cm^3/g)	D [6] (nm)	Y [7] (%)
1	$AC_{3\text{-}600\text{-}2\text{-}70}$	483.6	65.0	13.4	0.31	0.20	2.5	50.6
2	$AC_{3\text{-}700\text{-}2\text{-}70}$	666.4	77.2	11.6	0.38	0.27	2.3	49.5
3	$AC_{3\text{-}800\text{-}2\text{-}70}$	1041.4	179.5	17.2	0.57	0.40	2.2	47.4
4	$AC_{3\text{-}900\text{-}2\text{-}70}$	1816.3	1229.9	67.7	1.26	0.26	2.8	35.6
5	$AC_{3\text{-}1000\text{-}2\text{-}70}$	1166.5	1118.6	95.9	1.23	0.01	4.2	20.5
6	$AC_{1\text{-}900\text{-}2\text{-}70}$	1481.6	432.3	29.2	0.86	0.48	2.3	43.1
7	$AC_{2\text{-}900\text{-}2\text{-}70}$	1564.6	573.1	36.6	0.95	0.46	2.4	38.6
8	$AC_{4\text{-}900\text{-}2\text{-}70}$	1567.8	506.2	32.2	0.98	0.49	2.5	32.3
9	$AC_{3\text{-}900\text{-}1\text{-}70}$	1458.1	346.3	23.8	0.83	0.52	2.3	36.9
10	$AC_{3\text{-}900\text{-}3\text{-}70}$	1586.8	497.0	31.3	0.94	0.50	2.4	33.5
11	$AC_{3\text{-}900\text{-}2\text{-}40}$	1402.6	396.8	28.3	0.81	0.47	2.3	32.7
12	$AC_{3\text{-}900\text{-}2\text{-}100}$	1528.6	517.5	33.6	0.89	0.47	2.3	38.2

1 AC: activated carbon; R: K_2CO_3 to KL_d ratio; T: activation temperature (°C); t: dwell time (h); and v: N_2 flow rate (cm^3/min); 2 A_{BET}: BET surface area of AC; 3 A_e: external surface area of AC; 4 V_t: total pore volume of AC; 5 V_{micro}: micropore volume of AC; 6 D: average pore diameter of AC; 7 Y: yield of AC.

The effects of the activation temperature on the surface area and the pore volume are also shown in Table 1 (entries 1 to 5). As the activation temperature was increased from 600 to 900 °C, the surface area increased from 483.6 to 1816.3 m^2/g. However, further increases in the activation temperature (from 900 to 1000 °C) led to a marked decrease in carbon surface area, from 1816.3 to 1166.5 m^2/g due to the micropores having been widened or (and) merged to mesopores and macropores. In addition, at low activation temperatures, such as 600 °C, the main pore structure of the AC is microporous. However, as the activation temperature was increased to 1000 °C, the proportion of mesopores increased up to 95.9%. This increase in the mesopore volume fraction at 1000 °C may be

a result of some micropores creating larger pores (merged or widened of micropores). When the activation temperature was increased from 600 to 1000 °C, the average pore diameter increased from 2.5 to 4.2 nm.

Figure 2 shows the nitrogen adsorption-desorption isotherms of ACs prepared at various temperatures. The N_2 uptake increased with the increase in activation temperature and reached a maximum at 900 °C. Increasing the activation temperature to 1000 °C resulted in a partial decrease in the N_2 uptake.

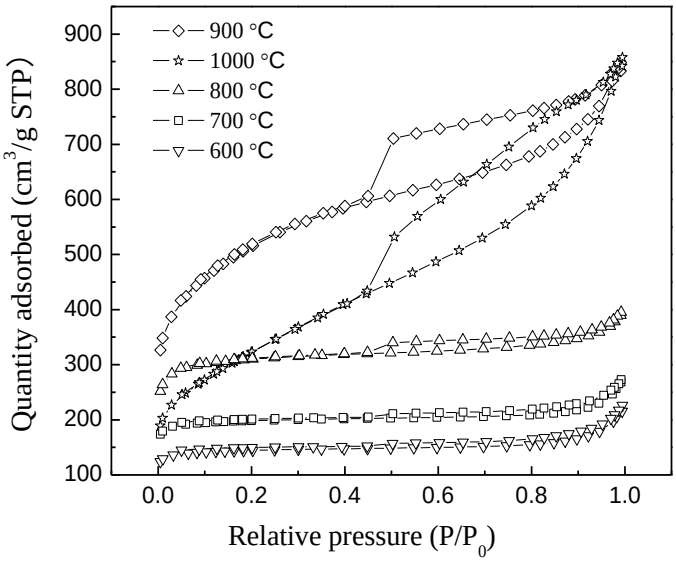

Fig. 2. Nitrogen adsorption isotherms of ACs obtained by K_2CO_3 at various activation temperatures (R = 3; t = 2 h; v = 70 cm^3/min)

In Fig. 2 no obvious hysteresis can be observed in the range 600 to 700 °C, indicating that the isotherms belonged to a type I of the IUPAC classification, characteristic of microporous materials. However, the isotherms at 900 and 1000 °C exhibited apparent hysteresis loops. This adsorption behavior is classified as a type IV isotherm, which implies that the ACs were highly mesoporous. This result indicates that the pore structure of the ACs could be tailored by controlling the activation temperature.

Figure 3 shows the pore size distributions of the ACs prepared from KL_d with different AT. ACs obtained at 600 to 800 °C suggested predominant micropores due to only slight incremental increases in mesoporous and macroporous volume. However, the ACs activated at 900 and 1000 °C have more mesopores and macroporous due to more incremental mesoporous and macroporous volume. This was in accordance with the results from the adsorption isotherms, as shown in Fig. 2.

The effect of the K_2CO_3/KL_d mass ratios on the carbon yield, BET surface area, and pore volumes is also shown in Table 1 (entries 4, 6, 7, and 8). The carbon yield decreased with increases in the K_2CO_3/KL_d mass ratio. This may be due to the higher the mass ratio of K_2CO_3/KL_d (the mass of KL_d is constant), the more K_2CO_3 reacted with carbon, and the more carbon was consumed, so that the yield of activated carbon decreased.

$$K_2CO_3+2C \rightarrow 2K+3CO \quad (3)$$

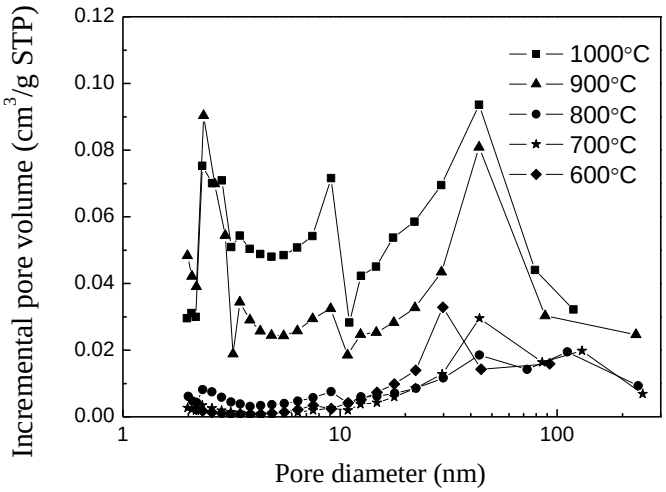

Fig. 3. Pore size distribution of ACs activated at various AT

As the mass ratios increased from 1 to 3, the BET surface area and pore volume also increased. This occurred because of an increase in the contact area between KL_d and the activating agent. This in turn increased the release of volatiles and the pore surface area. However, further increases in the mass ratio from 3 to 4 resulted in a decrease in the BET surface area and pore volume. This may be due to the higher K_2CO_3/KL_d mass ratio produce an extensive breaking of network structure of KL_d by alkali reagent, the shrinkage of the structure and consequently the reduction of the surface area and the total pore volume.

Figure 4 depicts the N_2 adsorption-desorption isotherms of ACs at various K_2CO_3/KL_d mass ratios. All isotherms displayed an abrupt increase in the adsorbed volume at a low relative pressure (P/P_0), indicating the presence of a large proportion of micropores. Furthermore, as the relative pressure increased to 0.4, the isotherms exhibited apparent hysteresis loops. This adsorption behavior exhibited a type IV isotherm, characteristic of mesoporous structure. Therefore, the ACs obtained at different K_2CO_3/KL_d mass ratios were both microporous and mesoporous in structure.

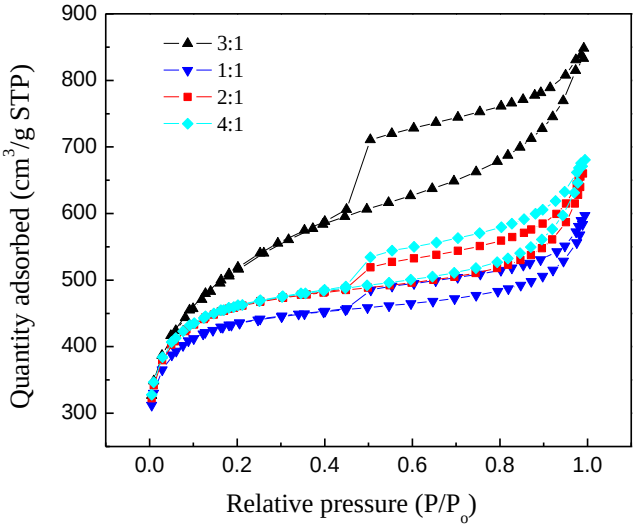

Fig. 4. Nitrogen adsorption isotherms of ACs obtained by a one-step activation method from various mass ratios of K_2CO_3 to KL_d (AT = 900 °C; t = 2 h; v = 70 cm^3/min)

The effects of the activation period on the carbon yield, BET surface area, and pore volumes are also shown in Table 1 (entries 4, 9, and 10). The carbon yield decreased slightly when the activation period was extended; this was primarily because of the promotion of carbon burn off and tar volatilization caused by a longer holding time. Both the S_{BET} and pore volumes of the resultant ACs increased slightly with increasing activation period up to 2 h. When the activation period was above 2 h, the S_{BET} decreased slightly from 1816.3 to 1586.8 m^2/g. This was because the excessive activation time led to the collapse of the pores; therefore, the surface area and pore volume became smaller. The results show that the 2-h activation period was a suitable length of time for carbon activation.

Figure 5 shows the pore characteristics of samples activated with K_2CO_3 at various activation periods. All isotherms exhibits a type IV isotherms with a pronounced desorption hysteresis loop, which is evidence of the presence of mesopores. Moreover, adsorption occurs at relatively low pressure, indicating the existence of micropores. These results indicate that the pore structure of ACs at various periods was both microporous and mesoporous.

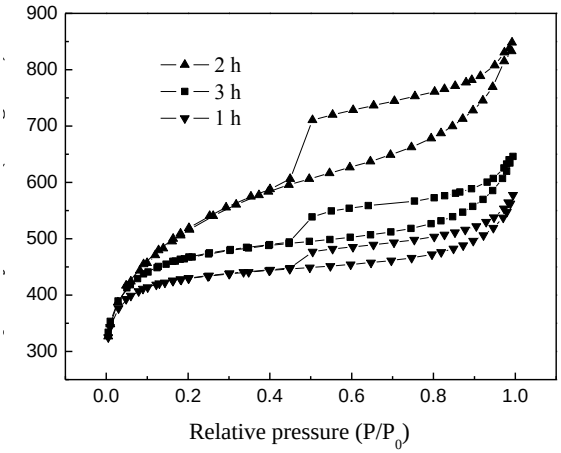

Fig. 5. Nitrogen adsorption isotherms of ACs obtained by a one-step activation method from various activation periods (AT = 900 °C; R = 3; v = 70 cm^3/min)

The effect of the N_2 flow rate on the yield, BET surface area, and pore volume is shown in Table 1 (entries 4, 11, and 12). The yield of ACs increased with increasing N_2 flow rate. A possible reason for this is that the activating agents, including water vapor, CO, and CO_2 formed under activation, were carried away rapidly by the high flow rate of inert gas (Foo and Hameed 2012). Therefore, the decrease of auxiliary activating agent with high N_2 flow rate resulted in the carbon consumption decreasing and carbon yield increasing. The surface area increased from 1402.6 to 1816.3 m^2/g and the pore volume increased from 0.81 to 1.26 cm^3/g, respectively, as the N_2 flow rate increased from 40 to 70 cm^3/min. However, the surface area and pore volume decreased to 1528.6 m^2/g and 0.89 cm^3/g, respectively, when the N_2 flow increased from 70 to 100 cm^3/min. Figure 6 shows the N_2 adsorption isotherms of the porous carbons prepared under various N_2 flow rates at 900 °C for 2 h. As can be seen in Fig. 6, all isotherms exhibit type IV mesoporous development but they also reveal microporous structure. At 70 cm^3/min N_2 flow rate, the mesoporosity was developed more than that of at 40 and 100 cm^3/min N_2 flow rate.

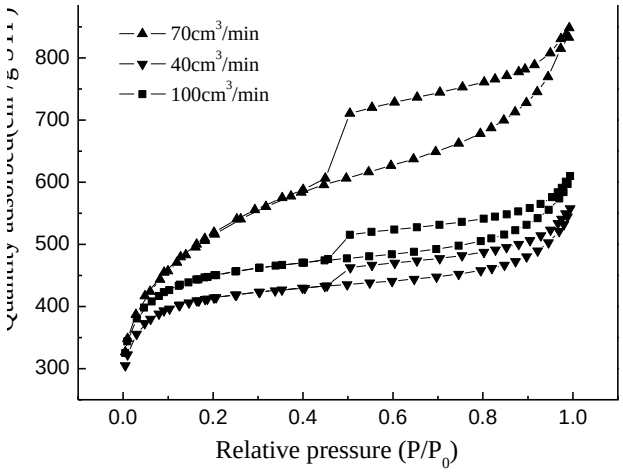

Fig. 6. Nitrogen adsorption isotherms of ACs obtained by a one-step activation method from various N_2 flow rates (AT = 900 ° C; *R* = 3; *t* = 2 h)

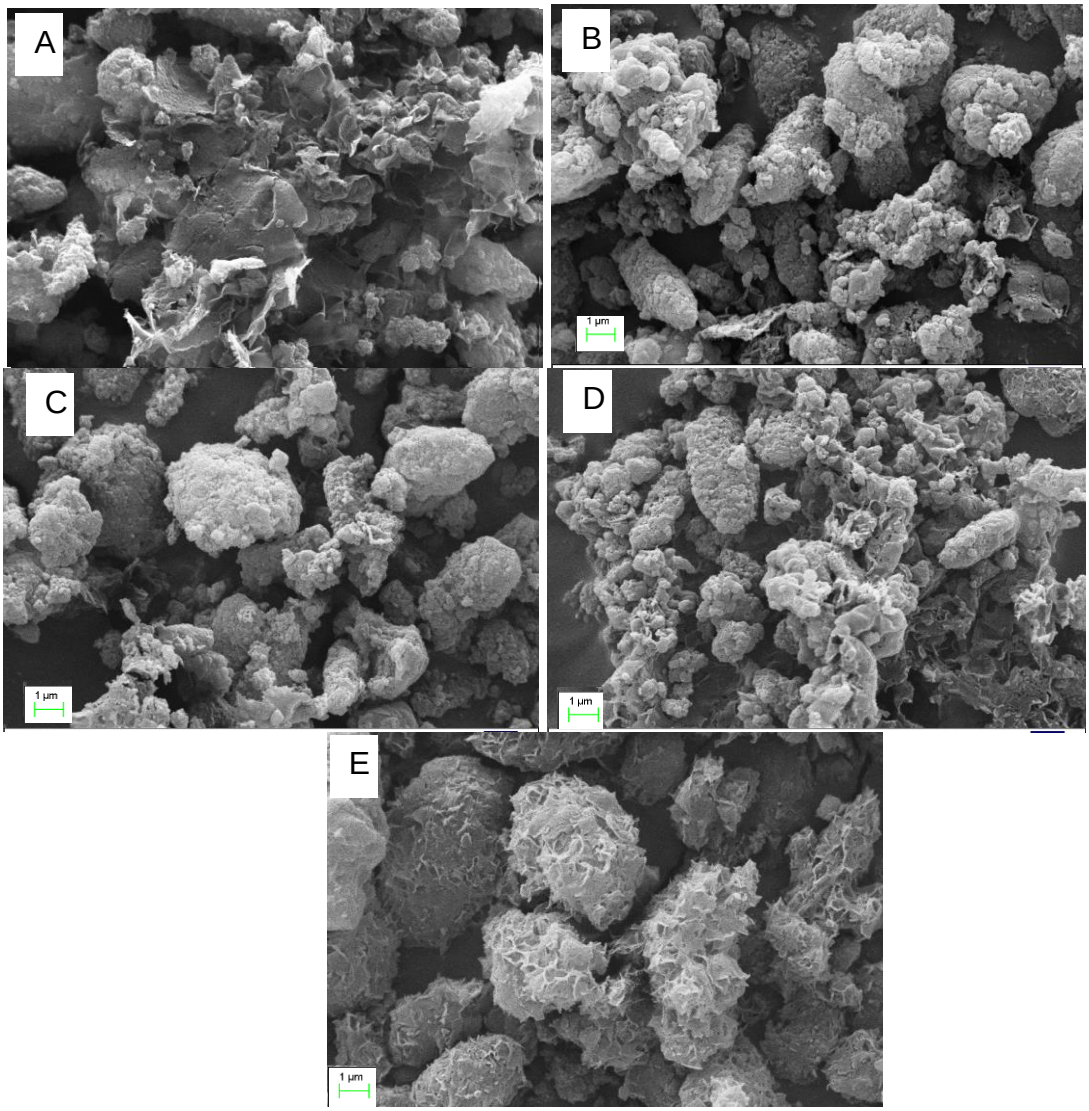

Fig. 7. SEM micrographs (20000×) of the ACs prepared by a one-step K_2CO_3 activation method at A) 600 °C, B) 700 °C, C) 800 °C, D) 900 °C, and E) 1000 °C (*R* = 3; *t* = 2 h; *v* = 70 cm^3/min)

SEM images of the ACs activated at various temperatures are shown in Fig. 7(a-e). There were observable differences between the 600 and 1000 °C ACs. The surfaces of the ACs obtained at 600 °C were smooth and without any pores. Nevertheless, the external surfaces of these ACs activated at 700 to 1000 °C showed rich porosities that were too small to be fully observed and were very irregular. The ACs obtained at 1000 °C had a notably different morphology than the ACs activated at 700 to 900 °C because the mesopores and macropores of these ACs resulted from the evaporation of K_2CO_3 during the 1000 °C carbonization, leaving behind spaces previously occupied by K_2CO_3.

Surface roughness is an important factor that influences the adsorption property of an adsorbent. The surface fractal dimension, based on the adsorption isotherm, is a measurement of surface roughness (Zhang *et al*. 2014b). The fractal FHH obtained from the isothermal data (relative pressure of 0 to 0.3) at various activated temperatures is plotted in Fig. 8. There was a good linear relationship between ln(ln(*P*/*P*)) and ln(*V*). The results show that the fractal dimensions obtained from fractal FHH were reliable.

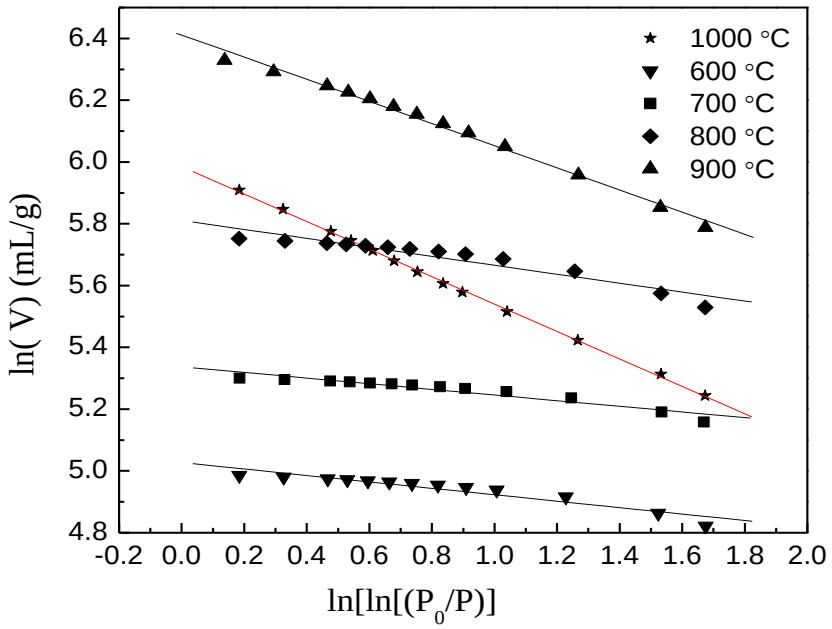

Fig. 8. Fractal FHH plots of ACs prepared from KL_d under various AT by K_2CO_3 activation

Figure 9 shows the influence of the activation temperature on the estimated fractal dimensions. The fractal dimensions of the ACs prepared by K_2CO_3 decreased with an increase in the activation temperature.

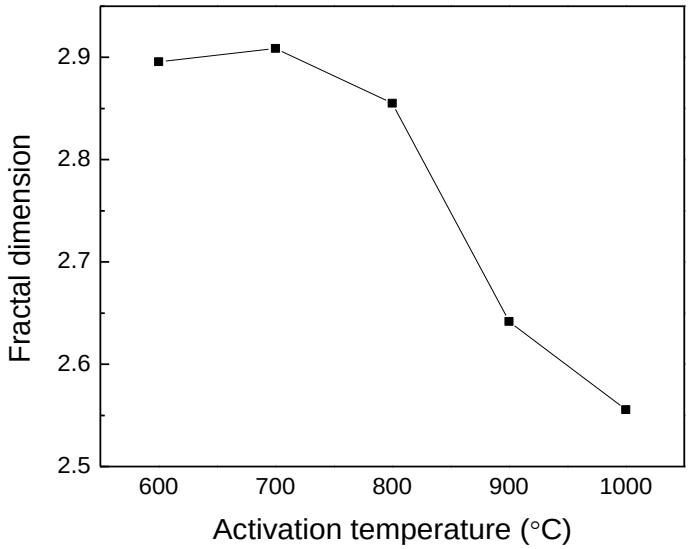

Fig. 9. Influence of activation temperature on the fractal dimensions of ACs

Comparing the fractal dimension with the mesopore proportion in Table 1 at different activation temperatures, the ACs activated at 700 °C exhibited the greatest fractal dimension and the smallest proportion of mesopores. At 1000 °C, the fractal dimension of AC was the smallest; however, it exhibited the greatest mesopore proportion at 95.9%. These results show that the fractal dimensions were consistent with the proportion of mesopores present. In other words, the fractal dimension decreased with increasing proportion of mesopores. This result is consistent with a previous report by Gómez-Serrano *et al*. (2005).

The recovery ratio of K_2CO_3 at various activation temperatures was investigated, and the results are shown in Fig. 10. The recovery ratio of K_2CO_3 decreased slightly between 600 and 800 °C, and decreased notably above 800 °C (Fig. 10). The results indicated that K_2CO_3 decomposed partially above 800 °C. By XRD characterization (not shown), the recovered K_2CO_3 and pure K_2CO_3 were found to have almost similar crystal structure, so the recovered activating agent can be reused in AC preparation.

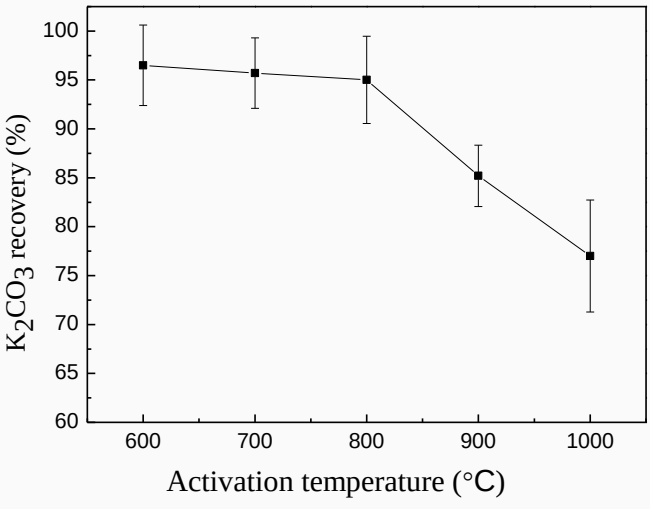

Fig. 10. Recovery ratio of K_2CO_3 at various activation temperatures

CONCLUSIONS

1. The preparation and characterization of activated carbon from kraft lignin was investigated in this work. In comparison to the K_2CO_3 to KL_d mass ratio, activation period, and N_2 flow rate, the carbonization temperature played the most crucial role in the amount of final product, the surface area, and the pore volume.
2. The prepared ACs attained a surface area of 1816.3 m^2/g, a total pore volume of 1.26 cm^3/g, and a high contribution of mesopores at 95.9% when the K_2CO_3 to KL_d mass ratio equaled 3, the activation temperature was 900 °C, the activation period was 2 h, and the N_2 flow rate was 70 cm^3/min.
3. The activating agent, K_2CO_3, can be partially recovered, and the washing water discharge can be minimized. From an economical and environmental standpoint, the use of a one-step chemical activation method is simple, efficient, low-cost, and environmentally friendly. This preparation method is suitable for large-scale, cleaner production of ACs with high mesoporous surface areas from KL by K_2CO_3 activation.

ACKNOWLEDGMENTS

This work was supported by the Research Projects of China Nuclear Facilities Decommissioning and Radioactive Waste Management (14ZG6101), the Key Project of Education Department of Sichuan Province (14ZA0092), and the Doctor Foundation of Southwest University of Science and Technology (14zx7155) and Innovation Team building fund project of Sichuan Provincial Biomass Modified Materials Engineering Research Center in China (14tdgc02).

REFERENCES CITED

Babeł, K., and Jurewicz, K. (2008). "KOH activated lignin based nanostructured carbon exhibiting high hydrogen electrosorption," *Carbon* 46, 1948-1956. DOI: 10.1016/j.carbon.2008.08.005

Bu, Q., Lei, H., Zacher, A. H., Wang, L., Ren, S., Liang, J., Wei, Y., Liu, Y., Tang, J., Zhang, Q., *et al.* (2012). "A review of catalytic hydrodeoxygenation of lignin-derived phenols from biomass pyrolysis," *Bioresource Technology* 124, 470-477. DOI: 10.1016/j.biortech.2012.08.089

Carrott, P. J. M., Suhas, Carrott, M. M. L. R., Guerrero, C. I., and Delgado, L. A. (2008). "Reactivity and porosity development during pyrolysis and physical activation in CO_2 or steam of kraft and hydrolytic lignins," *J. Anal. Appl. Pyrolysis* 82, 264-271. DOI:10.1016/j.jaap.2008.04.004

Fierro, V., Torné-Fernández, V., and Celzard, A. (2007). "Methodical study of the chemical activation of kraft lignin with KOH and NaOH," *Microporous & Mesoporous Materials* 101(3), 419-431. DOI: 10.1016/j.micromeso.2006.12.004

Foo, K.Y., and Hameed, B. H. (2012). "Preparation of activated carbon by microwave heating of langsat (*Lansium domesticum*) empty fruit bunch waste," *Bioresource Technology* 116, 522-525. DOI: 10.1016/j.biortech.2012.03.123

Foo, K.Y., and Hameed, B.H. (2011). "Utilization of rice husks as a feedstock for

preparation of activated carbon by microwave induced KOH and K_2CO_3 activation," *Bioresource Technology* 102, 9814-9817. DOI: 10.1016/j.biortech

Gómez-Serrano, V., Cuerda-Correa, E. M., Fernández-González, M. C., Alexandre-Franco, M. F., and Macías-García, A. (2005). "Preparation of activated carbons from walnut wood: A study of microporosity and fractal dimension," *Smart Materials & Structures* 14(2), 363-368. DOI: 10.1088/0964-1726/14/2/010

Hayashi, J., Muroyama, K., Gomes, V. G., and Watkinson, A. P. (2002). "Fractal dimensions of activated carbons prepared from lignin by chemical activation," *Carbon* 40(4), 630-632. DOI: 10.1016/S0008-6223(02)00017-9

Hayashia, J., Kazehayaa, A., Muroyamaa, K., and Watkinson, A. P. (2000). "Preparation of activated carbon from lignin by chemical activation," *Carbon* 38, 1873-1878.

Huang, L., Wang, M., Shi, C., Huang, J., and Zhang, B. (2014). "Adsorption of tetracycline and ciprofloxacin on activated carbon prepared from lignin with H_3PO_4 activation," *Desalination and Water Treatment* 52(13-15), 2678-2687. DOI: 10.1080/19443994.2013.833873

Jain, A., Balasubramanian, R., and Srinivasan, M. P. (2016). "Hydrothermal conversion of biomass waste to activated carbon with high porosity: A review," *Chemical Engineering Journal* 283, 789-805. DOI:10.1016/j.cej.2015.08.014

Kang, S., Li, X., Fan, J., and Chang, J. (2013). "Hydrothermal conversion of lignin: A review," *Renewable & Sustainable Energy Reviews* 27, 546-558. DOI: 10.1016/j.rser.2013.07.013

Lange, H., Decina, S., and Crestini, C. (2013). "Oxidative upgrade of lignin - Recent routes reviewed," *European Polymer Journal* 49(6), 1151-1173. DOI: 10.1016/j.eurpolymj.2013.03.002

Li, X. F., and Luo, X. G. (2015). "Preparation of mesoporous activated carbon supported Ni catalyst for deoxygenation of stearic acid into hydrocarbons," *Environmental Progress & Sustainable Energy* 34(2), 607-612. DOI:10.1002/ep.12026.

Li, X. F., Xu, Q., Fu, Y., and Guo, Q. X. (2014). "Preparation and characterization of activated carbon from kraft lignin via KOH activation," *Environmental Progress & Sustainable Energy* 33(2), 519-526. DOI: 10.1002/ep.11794

Liu, M., Chen, Y., Chen, K., Zhang, N., Zhao, X. Q., Zhao, F. H., Dou, Z. F., He, X. M., and Wang, L. (2015). "Biomass-derived activated carbon for rechargeable lithium-sulfur batteries," *BioResources* 10(1), 155-168. DOI: 10.15376/biores.10.1.155-168

Liu, Y., Guo, Y., Gao, W., Wang, Z., Ma, Y., and Wang, Z. (2012). "Simultaneous preparation of silica and activated carbon from rice husk ash," *Journal of Cleaner Production* 32, 204-209. DOI: 10.1016/j.jclepro.2012.03.021

Saha, D., Li, Y., Bi, Z., Chen, J., Keum, J. K., Dale, K., Hensley, D. K., Grappe, H. A., Meyer, III, H. M., Dai, S., Paranthaman, M. P., and Naskar, A. K. (2014). "Studies on supercapacitor electrode material from activated lignin-derived mesoporous carbon," *Langmuir* 30, 900-910. DOI:10.1021/la404112m

Song, X. H., Xu, R., Lai, A., Lo, H. L., Neo, F. L. and Wang, K. (2012). "Preparation and characterization of mesoporous activated carbons from waste tyre," *Asia-Pacific Journal of Chemical Engineering* 7, 474-478. DOI: 10.1002/apj.544

Suhas, Carrott, P. J. M., and Ribeiro Carrott, M. M. L. (2007). "Lignin - From natural adsorbent to activated carbon: A review," *Bioresource Technology* 98(12), 2301-2312. DOI: 10.1016/j.biortech.2006.08.008

Xia, H. Y., Peng, J. H., and Zhang, L. B. (2015). "Preparation of high surface area activated carbon from *Eupatorium adenophorum* using K_2CO_3 activation by

microwave heating," *Green Processing and Synthesis* 4(4), 299-305. DOI: 10.1515/gps-2015-0025

Zhang, J., Jin, X.J., Gao, J.M., and Zhang, X.D. (2014a). "Phenol adsorption on nitrogen-enriched activated carbon prepared from bamboo residues," *BioResources* 9(1), 969-983. DOI: 10.15376/biores.9.1.969-983

Zhang, S., Tang, S., Tang, D., Huang, W., and Pan, Z. (2014b). "Determining fractal dimensions of coal pores by FHH model: Problems and effects," *Journal of Natural Gas Science & Engineering* 21, 929-939. DOI: 10.1016/j.jngse.2014.10.018

Article submitted: June 29, 2015; Peer review completed: December 8, 2015; Revised version received: December 23, 2105; Accepted: December 24, 2015; Published: January 14, 2016.
DOI: 10.15376/biores.11.1.2096-2108